JOURNAL OF COMPUTATIONAL PHYSICS 73, 168–182 (1987)

Computation of MHD Equilibria by a Quasi-inverse Finite Hybrid Element Approach

R. GRUBER, R. IACONO, AND F. TROYON

Centre de Recherches en Physique des Plasmas,
Association Euratom–Confédération Suisse,
E'cole Polytechnique Fédérale de Lausanne,
21, av. des Bains, CH-1007 Lausanne, Switzerland

Received January 27, 1986; revised April 4, 1986

A quasi-inverse finite hybrid element code has been written to supply a precise and consistent solution of the Grad–Shafranov equation to the ideal linear MHD stability code ERATO. To fit the behavior at the plasma surface and in the region around the magnetic axis, adequate coordinate transformations are made. A Picard iteration is used to treat the nonlinearity of the source term. One Picard step is carried out by solving the weak form of the partial differential equation by an isoparametric finite hybrid element approach (FHE). After each Picard step, the nodal points are readjusted such that they fall on the initially prescribed flux surfaces. This enables us to accumulate the nodal points in those regions where good precision is needed for the stability code. While a 4-point integration is necessary for a conforming finite element scheme, a 1-point integration is sufficient in a FHE approach. Coding the FHE is very simple and easily vectorizable. For a given resolution, the precision of global quantities, such as the total flux, is the same for both methods but the FHE approach is faster.

1. INTRODUCTION

Finite difference and finite element methods approximate the exact solution Ψ of a second-order partial differential equation in the following way:

$$\|\Psi_h - \Psi\| < c\mathcal{O}(h^l), \tag{1}$$

where h and l represent the discretization mesh size and the order of the approximation, respectively. The value of the constant c strongly depends on the choice of the coordinate system and on how well the solution is approximated locally. For instance, c becomes large if the boundary is poorly represented.

To obtain a small $\|\Psi_h - \Psi\|$, one can choose between a high-order approach (l large), a fine grid (h small), and a formulation leading to a small value of c. However, the computational physicist is also concerned with the manpower necessary to achieve those goals, as well as the possibility of vectorizing the computer code. Often, these are sufficient reasons against high-order approaches. Also, high-order approaches can lead to the Gibbs phenomenon (parasitic overshoot

0021-9991/87 $3.00

oscillations) for solutions which vary rapidly in a localized region but are smooth elsewhere (see, for instance, Ref. [1]). In such situations, mesh accumulation helps to increase the precision of the approximate solution. For such cases a finite element method is preferable to a finite difference method where l decreases for a nonequidistant mesh. Besides h and l, the constant c in Eq. (1) plays an important role in the actual precision of the approximate solution Ψ_h. It is especially this constant that we try to keep small in our approach. We minimize the error of Ψ_h by:

(a) Choosing a coordinate system to represent the boundary as closely as possible and to fit the analytic behavior of the solution Ψ_h around particular points in the domain, particularly around the axis.

(b) Readjusting the grid iteratively to fit physically important surfaces.

(c) Accumulating the mesh around these surfaces.

(d) Choosing nonconforming isoparametric finite hybrid elements instead of conforming isoparametric elements to reduce a 4-point integration scheme to a 1-point integration formula. This reduces computing time of the matrix elements and eases vectorization.

This proceeding is applied to the fixed boundary Grad–Shafranov equation describing the equilibrium state of a thermonuclear tokamal fusion plasma (see Ref. [2]).

2. Physical Problem

2.1. *Equilibrium Equation*

In natural units [3] the static ideal MHD equilibrium equations are

$$\nabla p = (\nabla \times \mathbf{B}) \times \mathbf{B} \tag{2a}$$

$$\nabla \cdot \mathbf{B} = 0. \tag{2b}$$

Let us restrict consideration to axisymmetric geometry for which the toroidal angle ϕ is an ignorable coordinate (Fig. 1). For this geometry, Eq. (2b) is satisfied by

$$\mathbf{B} = T\nabla\phi + \nabla\phi \times \nabla\Psi. \tag{3}$$

By dotting Eq. (2a) with $\nabla\phi$ and $\mathbf{B}$, respectively, one finds that p and T are constant on constant-Ψ surfaces. Dotting Eq. (2a) with $\nabla\Psi$ gives the Grad–Shafranov equation in the plasma domain Φ,

$$r^2 \nabla \cdot \left(\frac{\nabla\Psi}{r^2} \right) = -r^2 \frac{dp}{d\Psi} - T\frac{dT}{d\Psi} = r\mathscr{S}(\Psi, r), \tag{4}$$

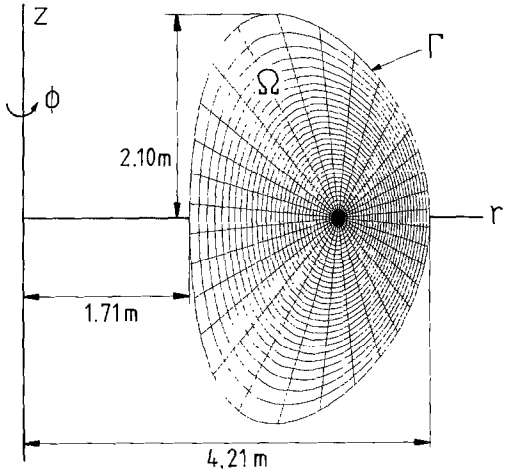

FIG. 1. The axisymmetric geometry for JET. Quasi-inverse solution $\alpha(\Psi, \theta)$ in the (r, z) plane using finite hybrid elements.

where r is the distance from the symmetry axis (see Fig. 1). We restrict ourselves to the fixed boundary problem for which

$$\Psi = 0 \tag{5}$$

at the plasma surface Γ.

To solve Eq. (4) one can prescribe two arbitrary functions $p(\Psi)$ and $T(\Psi)$. In general they are nonlinear functions in Ψ. In practice they are chosen such that $\mathcal{S}(\Psi, r) = 0$ at Γ and, as a consequence, the trivial solution $\Psi = 0$ satisfies (4) and (5). To avoid this particular solution, we have to normalize our system by demanding, for instance, that the total toroidal current

$$\int_\Omega r\nabla\phi \cdot (\nabla \times \mathbf{B})\, d^2x = \int_\Omega \mathcal{S}\, d^2x = I \tag{6}$$

be imposed. Here, d^2x is the area element in Ω. Condition (6) can be imposed by scaling the source

$$\mathcal{S} = \lambda \mathcal{S}^* \tag{7}$$

and solving for λ.

2.2. *Variational Form*

Introducing U to be the set of all functions $u \in L^2(\Omega)$,[1] $|\nabla u| \in L^2(\Omega)$, $u = 0$ at Γ, and $u < 0$ in Ω, problem equations (4)–(7) can be written in their weak form (see Ref. [4]):

[1] $L^2(\Omega)$ means: square integrable functions in Ω.

"Find a real number λ and $\Psi \in U$ such that

$$\int_\Omega \frac{1}{r} \nabla\Psi \cdot \nabla\eta d^2x + \lambda \int_\Omega \mathscr{S}^* d^2x = 0 \tag{8}$$

for all $\eta \in U$ such that for a given I

$$\lambda \int_\Omega \mathscr{S}^* d^2x = I."$$

2.3. *Coordinates to Fit Γ and Axis*

To fit the plasma surface precisely and to guarantee regularity at the magnetic axis, a new coordinate system (ϖ, θ) is introduced. It is related to the cylindrical coordinates (r, z) through

$$\begin{aligned} r &= R_0 + \sqrt{\varpi}\, \rho_\Gamma(\theta) \cos\theta \\ z &= \sqrt{\varpi}\, \rho_\Gamma(\theta) \sin\theta. \end{aligned} \tag{9}$$

The center of the coordinate system is given by $\varpi = 0$, corresponding to the point $(R_0, 0)$ in the (r, z) coordinate system. The plasma surface Γ is given by $\varpi = 1$. The given function $\rho_\Gamma(\theta)$ describes the form of Γ.

2.4. *Readjustment and Accumulation of the Mesh*

We iteratively readjust the grid to guarantee regularity of the solution at the magnetic axis and to fit the physically relevant $\Psi =$ constant surfaces. At the end of each Picard step the values of R_0 and ϖ are recalculated such that the point $r = R_0$, $z = 0$ falls on the minimum of Ψ in Ω and that the grid points $(\varpi_{ij}, \theta_j, j = 1, N_\theta)$ fall on prescribed Ψ_i surfaces. This makes it possible to accumulate the grid around singular Ψ surfaces, a procedure necessary to deliver a precise enough solution to the linear ideal MHD stability code ERATO. We call this a quasi-inverse approach.

3. Formulation of the Approximate Problem

3.1. *Picard Iteration*

The nonlinear problem (8) is solved iteratively by a Picard method. Let Ψ^k and λ^k be the approximate solution after k iteration steps. Then Ψ^{k+1} and λ^{k+1} are determined by:

"Find real numbers λ^{k+1} and $\Psi^{k+1} \in U$ such that[2]

$$\int_\Omega \frac{1}{r} \nabla\Psi^{k+1} \cdot \nabla\eta d^2x + \lambda^k \int_\Omega \mathscr{S}^{*k} \eta d^2x = 0 \tag{10}$$

[2] $\mathscr{S}^{*k}$ means: evaluate $\mathscr{S}^*$ using Ψ^k.

for all $\eta \in U$ and such that for a given value of I

$$\lambda^{k+1} \int_\Omega \mathscr{S}^{*k+1}\, d^2x = I."$$

As an initial guess for Ψ^0 one often takes a previously calculated solution in the same domain Ω with slightly different parameters in the source function. In most practical cases, the Picard method converges. In the few cases where it does not converge, a continuation method can be used (see Ref. [5]).

3.2. *Conforming Approximation*

Let us subdivide the domain Ω in $N_r \times N_z$ or $N_\alpha \times N_\theta$ mesh cells and let U_h be a finite-dimensional subspace of U. A Ritz–Galerkin method for approximating the eigenelements $(\Psi^{k+1}, \lambda^{k+1})$ of formulation (10) reduces to:

"Find real numbers λ_h^{k+1} and functions $\Psi_h^{k+1} \in U_h$ such that

$$\int_\Omega \frac{1}{r} \nabla \Psi_h^{k+1} \cdot \nabla \eta_h \, d^2x + \lambda_h^k \int_\Omega \mathscr{S}_h^{*k}\, \eta_h \, d^2x = 0 \tag{11}$$

for all $\eta_h \in U_h$ and such that for a given I

$$\lambda_h^{k+1} \int_\Omega \mathscr{S}_h^{*k+1}\, d^2x = I."$$

In (r, z) *coordinates* U_h is the set of all functions $u_h \in L^2(\Omega)$, $\partial u_h/\partial r \in L^2(\Omega)$, $\partial u_h/\partial z \in L^2(\Omega)$, $u_h = 0$ at Γ, and $u_h < 0$ in Ω. Formulation (11) then becomes:

"Find real numbers λ_h^{k+1} and functions $\Psi_h^{k+1} \in U_h$ such that

$$\int_\Omega \frac{1}{r} \left(\frac{\partial \Psi_h^{k+1}}{\partial r} \frac{\partial \eta_h}{\partial r} + \frac{\partial \Psi_h^{k+1}}{\partial z} \frac{\partial \eta_h}{\partial z} \right) dr\, dz + \lambda_h^k \int_\Omega \mathscr{S}_h^{*k}\, \eta_h \, dr\, dz = 0 \tag{12}$$

for all $\eta_h \in U_h$ and such that for a given I

$$\lambda_h^{k+1} \int_\Omega \mathscr{S}_h^{*k+1}\, dr\, dz = I."$$

In (α, θ) coordinates $Q = \{0 < \alpha < 1, \quad 0 \leqslant \theta \leqslant 2\pi\}$, $\Gamma = \{\alpha = 1, 0 \leqslant \theta \leqslant 2\pi\}$, and U_h is the set of all functions $u_h \in L^2(\Omega)$, $\partial u_h/\partial \alpha \in L^2(\Omega)$, $\partial u_h/\partial \theta \in L^2(\Omega)$, $u_h\ (\alpha = 1,\ \theta) = 0$, $u_h(\alpha, \theta) = u_h(\alpha, \theta + 2n\pi)$, where n is an integer and $u_h < 0$ in Ω. Formulation (11) then is:

"Find a real number λ_h^{k+1} and functions $\Psi_h^{k+1} \in U_h$ such that

$$\int_0^1 d\text{æ} \int_0^{2\pi} \frac{\text{æ}}{r}\left[\frac{\partial \Psi_h^{k+1}}{\partial \text{æ}}\frac{\partial \eta_h}{\partial \text{æ}} + \left(\frac{1}{2\text{æ}}\frac{\partial \Psi_h^{k+1}}{\partial \theta} - \frac{d\rho_I/d\theta}{\rho_I}\frac{\partial \Psi_h^{k+1}}{\partial \text{æ}}\right)\right.$$
$$\left.\times\left(\frac{1}{2\text{æ}}\frac{\partial \eta_h}{\partial \theta} - \frac{d\rho_I/d\theta}{\rho_I}\frac{\partial \eta_h}{\partial \text{æ}}\right)\right] d\theta$$
$$= \frac{1}{4}\lambda_h^k \int_0^1 d\text{æ} \int_0^{2\pi} \rho_I^2 \eta_h \mathscr{S}_h^{*k}\, d\theta \tag{13}$$

for all $\eta h \in U_h$ and for a given I

$$\frac{1}{2}\lambda_h^{k+1} \int_0^1 d\text{æ} \int_0^{2\pi} \rho_I^2 \mathscr{S}_h^{*k+1}\, d\theta = I."$$

3.3. *Nonconforming Approximation*

In addition to U_h, let us introduce three finite-dimensional spaces:

U_1 is the set of all functions $u_1 \in L^2(\Omega)$, such that u_1 $(\text{æ}=1, \theta)=0$, $u_1(\text{æ}, \theta) = u_1(\text{æ}, \theta + 2n\pi)$, where n is an integer and $u_1 < 0$ in Ω;

U_2 is the set of all functions $u_2 \in L^2(\Omega)$, such that $\partial u_2/\partial \text{æ} \in L^2(\Omega)$, u_2 $(\text{æ}=1, \theta)=0$, $u_2(\text{æ}, \theta) = u_2(\text{æ}, \theta + 2n\pi)$, where n is an integer and $u_2 < 0$ in Ω; and

U_3 is the set of all functions $u_3 \in L^2(\Omega)$, such that $\partial u_3/\partial \theta \in L^2(\Omega)$, u_3 $(\text{æ}=1, \theta)=0$, $u_3(\text{æ}, \theta) = u_3(\text{æ}, \theta - 2n\pi)$, where n is an integer and $u_3 < 0$ in Ω.

Formulation (13) can then be rewritten in a more complicated way:

"Find real numbers λ_h^{k+1} and functions $\Psi_h^{k+1} \in U_h$, $\Psi_1 \in U_1$, $\Psi_2 \in U_2$, and $\Psi_3 \in U_3$ such that[3]

$$\int_0^1 d\text{æ} \int_0^{2\pi} \frac{\text{æ}}{r}\left[\frac{\partial \Psi_2}{\partial \text{æ}}\frac{\partial \eta_2}{\partial \text{æ}} + \left(\frac{1}{2\text{æ}}\frac{\partial \Psi_3}{\partial \theta} - \frac{d\rho_I/d\theta}{\rho_I}\frac{\partial \Psi_2}{\partial \text{æ}}\right)\right.$$
$$\left.\times\left(\frac{1}{2\text{æ}}\frac{\partial \eta_3}{\partial \theta} - \frac{d\rho_I/d\theta}{\rho_I}\frac{\partial \eta_2}{\partial \text{æ}}\right)\right] d\theta$$
$$= \frac{1}{4}\lambda_h^k \int_0^1 d\text{æ} \int_0^{2\pi} \rho_I^2 \eta_1 \mathscr{S}_1^{*k}\, d\theta \tag{14}$$

for all $\eta_1 \in U_1$, $\eta_2 \in U_2$, $\eta_3 \in U_3$, such that

$$\int_0^1 d\text{æ} \int_0^{2\pi} (\Psi_h^{k+1} - \Psi_i)\,\zeta_i\, d\theta = 0, \qquad i = 1, 2, 3, \tag{15}$$

[3] $\mathscr{S}_1^{*k}$ means: evaluate $\mathscr{S}_1^{*k}$ using Ψ_1^k.

for all $\zeta_i \in L^2(\Omega)$, $i = 1, 2, 3$, and such that for a given I

$$\frac{1}{2}\lambda_h^{k+1}\int_0^1 d\alpha \int_0^{2\pi} \rho_r^2 \mathscr{S}_1^{*k+1}\, d\theta = I." \tag{16}$$

Note that formulations (13) and (14)–(16) are identical since the integral conditions (15) imply that

$$\Psi_i = \Psi_h^{k+1}, \qquad i = 1, 2, 3. \tag{17}$$

However, they differ if the functions ζ_i, $i = 1, 2, 3$, are chosen in a finite-dimensional function space.

4. Lowest-Order Finite Elements

4.1. *Choice of Finite Elements*

In a first step we subdivide the domain $\Omega = \{0 < \alpha < 1,\ 0 \leqslant \theta \leqslant 2\pi\}$ into $N_\alpha \times N_\theta$ rectangular mesh cells. As functions η_h, η_1, η_2, η_3, ζ_1, ζ_2, and ζ_3 we choose bilinear finite elements defined by $(i = 1, \ldots, N_\alpha; j = 1, \ldots, N_\theta)$

$$\begin{aligned}
\eta_h &= e_i(\alpha) \cdot e_j(\theta) \\
\eta_1 &= c_{i-1/2}(\alpha) \cdot c_{j-1/2}(\theta) \\
\eta_2 &= e_i(\alpha) \cdot c_{j-1/2}(\theta) \\
\eta_3 &= c_{i-1/2}(\alpha) \cdot e_j(\theta) \\
\zeta_1 = \zeta_2 &= \zeta_3 = c_{i-1/2}(\alpha) \cdot c_{j-1/2}(\theta).
\end{aligned} \tag{18}$$

The finite elements $c_{k-1/2}(x)$ and $e_k(x)$ are

$$\begin{aligned}
c_{k-1/2}(x) &= 0, && x_0 < x < x_{k-1} \\
&= 1, && x_{k-1} < x < x_k \\
&= 0, && x_k < x < x_N
\end{aligned} \tag{19}$$

$$\begin{aligned}
e_k(x) &= 0, && x_0 < x < x_{k-1} \\
&= \frac{x - x_{k-1}}{x_k - x_{k-1}}, && x_{k-1} < x \leqslant x_k \\
&= \frac{x_{k+1} - x}{x_{k+1} - x_k}, && x_k \leqslant x < x_{k+1} \\
&= 0, && x_{k+1} < x < x_N.
\end{aligned} \tag{20}$$

The unknowns Ψ_h^{k+1}, Ψ_1, Ψ_2, and Ψ_3 are expanded in terms of the finite elements

$$\begin{aligned}
\Psi_h^{k+1}(\varkappa, \theta) &= \sum_{i=0}^{N_\varkappa - 1} \sum_{j=0}^{N_\theta} \Psi_{i,j}\, e_i(\varkappa)\, e_j(\theta) \\
\Psi_1(\varkappa, \theta) &= \sum_{i=1}^{N_\varkappa} \sum_{j=1}^{N_\theta} \Psi_{i-1/2,\,j-1/2}\, c_{i-1/2}(\varkappa)\, c_{j-1/2}(\theta) \\
\Psi_2(\varkappa, \theta) &= \sum_{i=0}^{N_\varkappa - 1} \sum_{j=1}^{N_\theta} \Psi_{i,j-1/2}\, e_i(\varkappa)\, c_{j-1/2}(\theta) \\
\Psi_3(\varkappa, \theta) &= \sum_{i=1}^{N_\varkappa} \sum_{j=0}^{N_\theta} \Psi_{i-1/2,\,j}\, c_{i-1/2}(\varkappa)\, e_j(\theta).
\end{aligned} \tag{21}$$

When bilinear finite elements (Eqs. (21)) are chosen to represent Ψ_h^{k+1}, the integrals in the formulation (13) have to be performed by a 4-point Gauss formula.

4.2. *Conforming Isoparametric Finite Elements*

Let us now discretize the domain Ω into $N_\varkappa \times N_\theta$ quadrangular (nonrectangular) mesh cells. In this case we have to perform local variable transformations $(\varkappa, \theta) \to (\xi, \chi)$ of the form

$$\begin{aligned}
\varkappa(\xi, \chi) &= \alpha_1 + \alpha_2 \xi + \alpha_3 \chi + \alpha_4 \xi\chi \\
\theta(\xi, \chi) &= \beta_1 + \beta_2 \xi + \beta_3 \chi + \beta_4 \xi\chi.
\end{aligned} \tag{22}$$

The eight parameters α_1 to α_4 and β_1 to β_4 are determined by the coordinates $\varkappa_1$ to $\varkappa_4$ and θ_1 to θ_4 (see Fig. 2):

$$\begin{aligned}
\alpha_1 &= \varkappa_1, & \beta_1 &= \vartheta_1 \\
\alpha_2 &= \varkappa_2 - \varkappa_1, & \beta_2 &= \vartheta_2 - \vartheta_1 \\
\alpha_3 &= \varkappa_4 - \varkappa_1, & \beta_3 &= \vartheta_4 - \vartheta_1 \\
\alpha_4 &= \varkappa_1 + \varkappa_3 - \varkappa_2 - \varkappa_4, & \beta_4 &= \vartheta_1 + \vartheta_3 - \vartheta_2 - \vartheta_4.
\end{aligned} \tag{23}$$

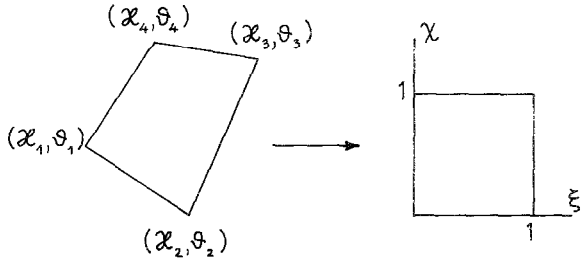

FIG. 2. Transformation from a quadrangular cell in the $(\varkappa, \theta)$ plane to a unit square in the (ξ, χ) plane.

In order to prevent problems concerning integration and uniqueness of the transformation (23), we demand that all angles of the quadrangles be smaller than π.

By transforming from (α, θ) to (ξ, χ), the surface element becomes

$$d\alpha\, d\theta = J d\xi\, d\chi\,, \tag{24}$$

where

$$J = \frac{1}{\dfrac{\partial \xi}{\partial \alpha}\dfrac{\partial \chi}{\partial \theta} - \dfrac{\partial \xi}{\partial \theta}\dfrac{\partial \chi}{\partial \alpha}} = (\alpha_2 + \alpha_4 \chi)(\beta_3 + \beta_4 \xi) - (\beta_2 + \beta_4 \chi)(\alpha_3 + \alpha_4 \xi) \tag{25}$$

is the Jacobian. In these new (ξ, χ) coordinates the derivatives of any quantity A become

$$\begin{aligned} J\frac{\partial A}{\partial \alpha} &= (\beta_3 + \beta_4 \xi)\frac{\partial A}{\partial \xi} - (\beta_2 + \beta_{4\chi})\frac{\partial A}{\partial \chi} \\ J\frac{\partial A}{\partial \theta} &= -(\alpha_3 + \alpha_4 \xi)\frac{\partial A}{\partial \xi} + (\alpha_2 + \alpha_{4\chi})\frac{\partial A}{\partial \chi}. \end{aligned} \tag{26}$$

One has to note that these formulae are still valid when the quadrangle degenerates into a triangle as can happen at the origin of a cylindrical coordinate system.

The finite elements now have to be constructed in such a way that $c_{k-1/2}(x)$ be piecewise constant in ξ or χ and that $e_k(x)$ be linear in ξ or in χ. The precise functional dependences of the elements in the (α, θ) plane can be found through the transformation (22).

In practice, one knows the coordinates α and θ of the four edge points of a cell. These define the transformation equations (23) and, consequently, the Jacobian through Eq. (25). The 4-point Gauss integration is performed in the (ξ, χ) plane. A back-transformation is necessary to determine the positions of the Gauss points in the (α, θ) plane.

4.3. *Non conforming Isoparametric Finite Hybrid Elements*

Let us first consider the case of a rectangular (α, θ) mesh. Choosing the elements of Eqs. (18) for η_h, $\eta_1, \eta_2, \eta_3, \zeta_1, \zeta_2$, and ζ_3 and the expansion equations (21) for Ψ_h^{k+1}, Ψ_1, Ψ_2, and Ψ_3, the integral conditions (Eqs. (15)), in the formulation given by Eqs. (14)–(16), correspond to

$$\begin{aligned} \Psi_{i-1/2,j-1/2} &= \tfrac{1}{4}(\Psi_{i-1,j-1} + \Psi_{i,j-1} + \Psi_{i-1,j} + \Psi_{i,j}) \\ \Psi_{i,j-1/2} &= \tfrac{1}{2}(\Psi_{i,j-1} + \Psi_{i,j}) \\ \Psi_{i-1/2,j} &= \tfrac{1}{2}(\Psi_{i-1,j} + \Psi_{i,j}). \end{aligned} \tag{27}$$

As a consequence, the derivatives of Ψ_2 with respect to α and Ψ_3 with respect to θ become centered finite differences

$$\frac{\partial \psi_2}{\partial \alpha}(\alpha_{i-1/2,j-1/2}, \vartheta_{i-1/2,j-1/2}) = \frac{\psi_{i,j-1}+\psi_{i,j}-\psi_{i-1,j-1}-\psi_{i-1,j}}{2(\alpha_{i,j}-\alpha_{i-1,j-1})}$$

$$\frac{\partial \psi_3}{\partial \vartheta}(\alpha_{i-1/2,j-1/2}, \vartheta_{i-1/2,j-1/2}) = \frac{\psi_{i,j}+\psi_{i-1,j}-\psi_{i,j-1}-\psi_{i-1,j-1}}{2(\vartheta_{i,j}-\vartheta_{i-1,j-1})}. \tag{28}$$

It is for this reason that we originally called this non-conforming approach a "finite hybrid element method."

All the quantities in Eqs. (14) and (16) including η and Ψ are now piecewise constant in each mesh cell. If, in each mesh cell, we approximate all the coefficients, i.e., α, ρ_Γ, and $d\rho_\Gamma/d\theta$, by their values at the center of the cell, the integrals in Eqs. (14) and (16) simply become

$$\int_0^1 d\alpha \int_0^{2\pi} A(\alpha, \vartheta)\, d\vartheta$$

$$= \sum_{i=1}^{N_\alpha} \sum_{j=1}^{N_\vartheta} A(\alpha_{i-1/2,j-1/2}, \vartheta_{i-1/2,j-1/2})(\alpha_{i,j}-\alpha_{i-1,j})(\vartheta_{i,j}-\vartheta_{i,j-1}). \tag{29}$$

Let us now consider the case of a quadrangular, i.e., nonrectangular mesh. Again we perform a local variable transformation as given by Eqs. (22). Again choosing all the quantities to be piecewise constant in a (ξ, χ) cell, a one-point integration formula is again sufficient and can be written directly in the (α, θ) plane as

$$\int_0^1 d\alpha \int_0^{2\pi} A(\alpha, \vartheta)\, d\vartheta = \sum_{i=1}^{N_\alpha} \sum_{j=1}^{N_\vartheta} A(\bar{\alpha}_{i-1/2,j-1/2}, \bar{\vartheta}_{i-1/2,j-1/2})\, J_{i-1/2,j-1/2},$$

where

$$\begin{aligned}
\bar{\alpha}_{i-1/2,j-1/2} &= \tfrac{1}{4}(\alpha_{i-1,j-1}+\alpha_{i,j-1}+\alpha_{i-1,j}+\alpha_{i,j}) \\
\bar{\vartheta}_{i-1/2,j-1/2} &= \tfrac{1}{4}(\vartheta_{i-1,j-1}+\vartheta_{i,j-1}+\vartheta_{i-1,}+\vartheta_{i,j}) \\
J_{i-1/2,j-1/2} &= \tfrac{1}{2}[(\vartheta_{i-1,j}-\vartheta_{i,j-1})(\alpha_{i,j}-\alpha_{i-1,j-1}) \\
&\quad +(\vartheta_{i,j}-\vartheta_{i-1},j-1)(\alpha_{i,j-1}-\alpha_{i-1,j})].
\end{aligned} \tag{30}$$

The quantities that contain Ψ in Eq. (14) become

$$\psi_1(\bar{\alpha}_{i-1/2,j-1/2}, \bar{\vartheta}_{i-1/2,j-1/2}) = \frac{1}{4}(\psi_{i-1,j-1}+\psi_{i,j-1}+\psi_{i-1,j}+\psi_{i,j})$$

$$\begin{aligned}
\frac{\partial \psi_2}{\partial \alpha}(\bar{\alpha}_{i-1/2,j-1/2}, \bar{\vartheta}_{i-1/2,j-1/2}) &= \frac{1}{2J_{i-1/2,j-1/2}}[(\vartheta_{i-1,j}-\vartheta_{i,j-1})(\psi_{i,j}-\psi_{i-1,j-1}) \\
&\quad +(\vartheta_{i,j}-\vartheta_{i-1,j-1})(\psi_{i,j-1}-\psi_{i-1,j})]
\end{aligned} \tag{31}$$

$$\begin{aligned}
\frac{\partial \psi_3}{\partial \vartheta}(\bar{\alpha}_{i-1/2,j-1/2}, \bar{\vartheta}_{i-1/2,j-1/2}) &= \frac{1}{2J_{i-1/2,j-1/2}}[(\alpha_{i,j-1}-\alpha_{i-1,j})(\psi_{i,j}-\psi_{i-1,j-1}) \\
&\quad +(\alpha_{i-1,j-1}-\alpha_{i,j})(\psi_{i,j-1}-\psi_{i-1,j})].
\end{aligned}$$

For the test functions η, one has to take the values at the center of the (ξ, χ) cells and transform them back to the (α, θ) plane. The test functions attributed to the four nodal values $\Psi_{i-1,j-1}$, $\Psi_{i,j-1}$, $\Psi_{i-1,j}$, Ψ_{ij} in the mesh cell are

$$\eta_1 = (\tfrac{1}{4}, \tfrac{1}{4}, \tfrac{1}{4}, \tfrac{1}{4})$$

$$\frac{\partial \eta_2}{\partial \alpha} = \left(-\frac{\vartheta_{i-1,j} - \vartheta_{i,j-1}}{2J_{i-1/2,j-1/2}}, \frac{\vartheta_{i,j} - \vartheta_{i-1,j-1}}{2J_{i-1/2,j-1/2}}, -\frac{\vartheta_{i,j} - \vartheta_{i-1,j-1}}{2J_{i-1/2,j-1/2}}, \frac{\vartheta_{i-1,j} - \vartheta_{i,j-1}}{2J_{i-1/2,j-1/2}} \right) \tag{32}$$

$$\frac{\partial \eta_3}{\partial \alpha} = \left(\frac{\alpha_{i-1,j} - \alpha_{i,j-1}}{2J_{i-1/2,j-1/2}}, -\frac{\alpha_{ij} - \alpha_{i-1,j-1}}{2J_{i-1/2,j-1/2}}, \frac{\alpha_{i,j} - \alpha_{i-1,j-1}}{2J_{i-1/2,j-1/2}}, -\frac{\alpha_{i-1,j} - \alpha_{i,j-1}}{2J_{i-1/2,j-1/2}} \right).$$

A practical application of the use of finite hybrid elements is presented in Ref. [1] with the corresponding computer code for the case of the linear ideal MHD stability code ERATO in toroidal geometry.

5. Results

5.1. *Solov'ev Equilibrium*

Let us first compare the conforming and the nonconforming hybrid element approaches using the analytic Solov'ev equilibrium solution given by

$$\frac{dp}{d\Psi} = -2\Psi_s(1+E^2)/a^2E^2$$
$$\frac{dT^2}{d\Psi} = 0 \tag{33}$$

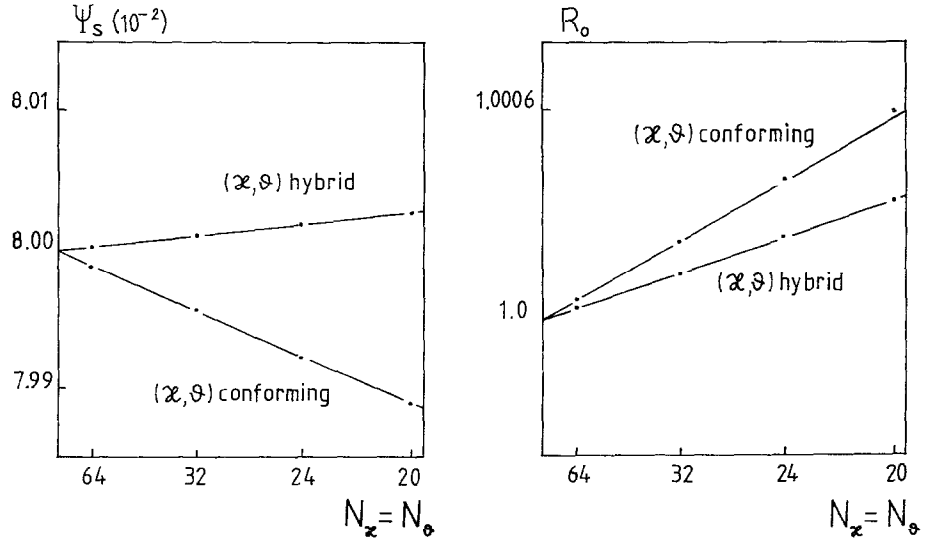

FIG. 3. Convergence studies for the total poloidal flux Ψ_s and the position of the magnetic axis R_0 for the conforming and finite hybrid element approaches. A straight line means quadratic convergence. Its slope defines c. Solov'ev equilibrium: $E = 1$, $a = 0.4$, $dp/d\Psi = -2$. The analytic values are $\Psi_s = 0.08$ and $R_0 = 1$.

with the surface parametrization $\rho_I(\theta)$ determined from

$$a^2 = E^{-2}(1+\rho_I(\theta)\cos\theta)^2\,\rho_I^2(\theta)\sin^2\theta + 0.25(2+\rho_I(\theta)\cos\theta)^2\,\rho_I^2(\theta)\cos^2\theta. \tag{34}$$

Here, a, E, and Ψ_s denote the inverse aspect ratio, the elongation, and the total flux. The position of the magnetic axis is at $r = R_0 = 1$. Note that $\rho_I(0) = \sqrt{1+2a} - 1$ and $\rho_I(\pi) = 1 - \sqrt{1-2a}$.

In Fig. 3 we show convergence studies of the approximated solutions corresponding to the set of parameters $a = 0.4$, $E = 1$, and $dp/d\Psi = -2$. We see that both methods, the conforming and the hybrid finite elements, converge quadratically toward the exact values of $\Psi_s = 0.08$ and $R_0 = 1$, the slope of the convergence curve for the hybrid elements being smaller. This means that the value of c in Eq. (1) is smaller for the nonconforming approach than for the conforming one.

For the case with $a = 0.4$, $E = 2$, and $dp/d\Psi = -2.5$, we see in Fig. 4 that the conforming approach has convergence behavior similar to that of the hybrid one. In Fig. 5 we show the convergence behavior of the quantity Ψ_s fixing either $N_\alpha = 20$ or $N_\theta = 20$. The error for $N_\alpha = 20$ is much smaller than that for $N_\theta = 20$. We find that N_θ of the order of $\sim 3N_\alpha$ is necessary for a balanced convergence study. The different convergence behaviors are due to the choice of nonconforming finite hybrid elements.

Fixing the elongation at $E = 2$ and $dp/d\Psi = -2.5$ and increasing the aspect ratio such that $a = 0.25$ makes the convergence properties of the conforming approach

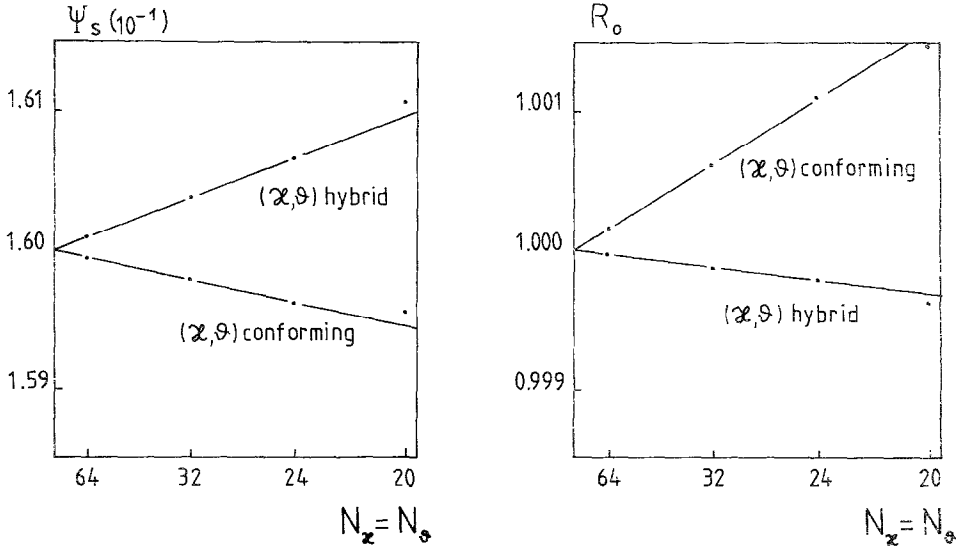

FIG. 4. Convergence studies for Ψ_s and R_0 for the conforming and finite hybrid element approaches. Solov'ev equilibrium: $E = 2$, $A = 0.4$, $dp/d\Psi = -2.5$. The analytic values are $\Psi_s = 0.16$ and $R_0 = 1$.

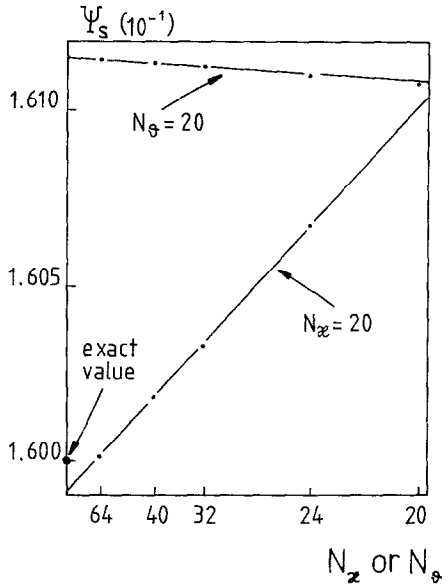

FIG. 5. Finite hybrid elements: convergence studies in N_ϑ for fixed $N_\chi = 20$ and in N_χ for fixed $N_\vartheta = 20$.

superior to those of the hybrid approach as we can see in Fig. 6. This is due to the superior integration formula (4-point Gauss integration formula) used for the conforming elements which allows a better representation of the plasma surface term

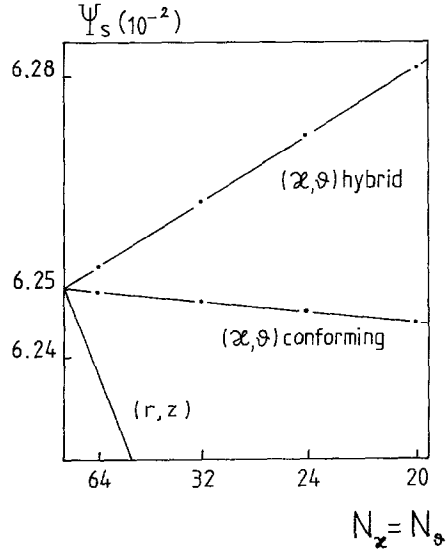

FIG. 6. Convergence studies for Ψ_s for the conforming and finite hybrid element approaches. Solov'ev equilibrium: $E = 2$, $a = 0.25$, $dp/d\Psi = -2.5$. The analytic value is $\Psi_s = 0.0625$.

containing $(d\rho_\Gamma/d\theta)/\rho$ in Eq. (13). Comparing these results with those presented in Ref. [4] using (r, z) coordinates (Eq. (12)), one realizes that 3 to 10 times fewer intervals have to be taken in both directions to obtain the same precision when using (ϖ, θ) coordinates.

5.2. *JET Equilibrium*

As a practical application we calculate the equilibrium solution for a JET (Joint European Torus) geometry. The parameters of the JET tokoamak are $R_0 = 2.96$ m, $a = 0.423$, $T = 10.4$ Tm, $E = 1.68$, and $I = 4.8 \times 10^6$ A. For the two free functions of the source term we choose

$$\begin{aligned} p(\psi/\psi_s) &= 38.1\ (\psi/\psi_s)^2 - 5.2\ (\psi/\psi_s)^3\ \mathrm{N/cm^2} \\ T^2\ (\psi/\psi_s) &= 110 - 2.85(\psi/\psi_s)^2\ T^2 m^2, \end{aligned} \tag{35}$$

which correspond to a case with $\beta = 2.5\%$, close to the Troyon stability limit [1,6]. The plasma surface Γ is D-shaped and given by

$$\begin{aligned} r_\Gamma &= 2.96\ (1 + a\cos(\theta + 0.3\sin\theta))\ m \\ z_\Gamma &= 2.96 \cdot E\, a \sin\theta\ m. \end{aligned} \tag{36}$$

The quasi-inverse solution $\varpi(\Psi, \theta)$, found by adjusting ϖ such that the grid points fall on $\Psi =$ constant surfaces, is represented in the (r, z) plane in Fig. 1. The convergence properties for the conforming and finite hybrid element approaches are shown in Fig. 7. As for the Solov'ev case, the finite hybrid elements have at least as good convergence properties as the conforming elements.

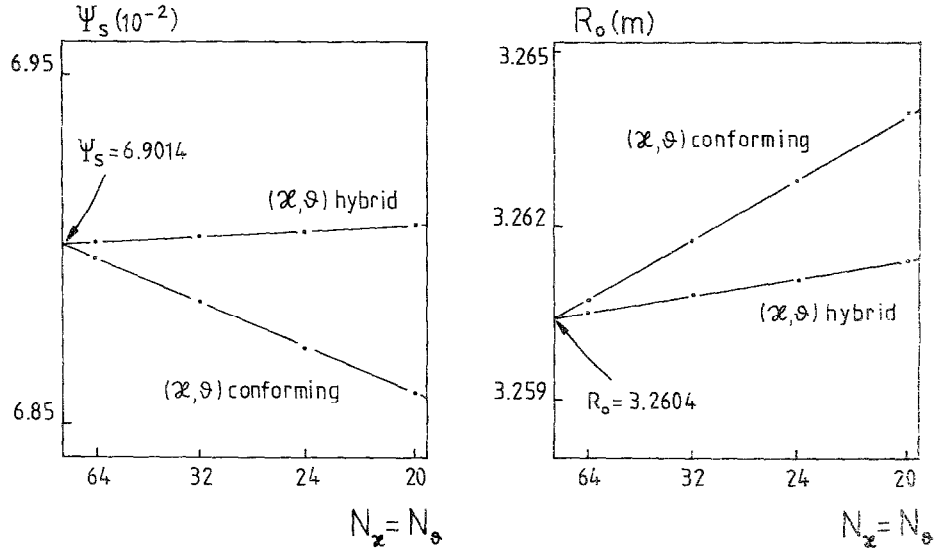

FIG. 7. JET geometry: convergence studies for Ψ_s and R_0 for conforming and finite hybrid element approaches.

Moreover, for a given resolution, the calculation of an equilibrium using hybrid elements is about two times faster than using a conforming approach.

6. Conclusions

We have compared two finite element approaches, the conforming and a nonconforming one, by applying them to the Grad–Shafranov equation. It is found that the nonconforming finite hybrid element approach shows better convergence behavior in most cases for the global quantities such as total flux or position of the magnetic axis. This hybrid approach is easier to implement and only needs a one-point integration formula for the calculation of the matrix elements. As a consequence, a relevant gain in computing time is obtained and the full vectorization of the matrix construction is simplified. After their success in the stability problem (Ref. [1]), the hybrid elements have also shown their superiority to the conforming elements in the calculation of ideal fixed boundary MHD equilibria.

References

1. R. Gruber and J. Rappaz, *Finite Element Methods in Linear Ideal Magnetohydrodynamics*, Springer Series in Computational Physics (Springer-Verlag, New York/Berlin, 1985).
2. *Proceedings, 2nd European Workshop on Computational Problems in the Calculation of* MHD *Equilibria (Wildhaus, 12–14 September 1983)*, published in *Comput. Phys. Commun.* **31**, 115 (1984); *Comput. Phys. Rep.* **1**, 345 (1984); L. M. Degtyarev and V. V. Drozdov, *Comput. Phys. Rep.* **2**, 341 (1985).
3. E. S. Weibel, *Amer. J. Phys.* **36**, 1130 (1968).
4. S. Semenzato, R. Gruber, and H. P. Zehrfeld, *Comput. Phys. Rep.* **1**, 389 (1984).
5. J. Blum, J. Le Foll, and B. Thorris, *Comput. Phys. Commun.* **24**, 235 (1981).
6. F. Troyon, R. Gruber, H. Saurenmann, S. Semenzato, and S. Succi, *Plasma Phys.* **26** (1A), 209 (1983).